High resolution and dynamic imaging of biopersistence and bioreactivity of extra and intracellular MWNTs exposed to microglial cells

Angela E. Goode[1*], Daniel A. Gonzalez Carter[2], Michael Motskin[2], Ilse S. Pienaar[2], Shu Chen[1], Sheng Hu[3], Pakatip Ruenraroengsak[1], Mary P. Ryan[1], Milo S. P. Shaffer[3], David T. Dexter[2], Alexandra E. Porter[1*].

1. Department of Materials, Imperial College London, Exhibition Road, London, SW7 2AZ, UK
2. Centre for Neuroinflammation and Neurodegeneration, Department of Medicine, Division of Brain Sciences, Imperial College London, London, W12 0NN, UK
3. Department of Chemistry, Imperial College London, Exhibition Road, London, SW7 2AZ, UK

*aeg08@ic.ac.uk

*a.porter@imperial.ac.uk

Abstract

Multi-walled carbon nanotubes (MWNTs) are increasingly being developed both as neuro-therapeutic drug delivery systems to the brain and as neural scaffolds to drive tissue regeneration across lesion sites. MWNTs with different degrees of acid oxidation may have different bioreactivities and propensities to aggregate in the extracellular environment, and both individualised and aggregated MWNTs may be expected to be found in the brain. Before practical application, it is vital to understand how both aggregates and individual MWNTs will interact with local phagocytic immune cells, the microglia, and ultimately to determine their biopersistence in the brain. The processing of extra- and intracellular MWNTs (both pristine and when acid oxidised) by microglia was characterised across multiple length scales by correlating a range of dynamic, quantitative and multi-scale techniques, including: UV-vis spectroscopy, light microscopy, focussed ion beam scanning electron microscopy and transmission electron microscopy. Dynamic, live cell imaging revealed the ability of microglia to break apart and internalise micron-sized extracellular agglomerates of acid oxidised MWNT, but not pristine MWNTs. The total amount of MWNTs internalised by, or strongly bound to, microglia was quantified as a function of time. Neither the significant

uptake of oxidised MWNTs, nor the incomplete uptake of pristine MWNTs affected microglial viability, pro-inflammatory cytokine release or nitric oxide production. However, after 24 hrs exposure to pristine MWNTs, a significant increase in the production of reactive oxygen species was observed. Small aggregates and individualised oxidised MWNTs were present in the cytoplasm and vesicles, including within multilaminar bodies, after 72 hours. Some evidence of morphological damage to oxidised MWNT structure was observed including highly disordered graphitic structures, suggesting possible biodegradation. This work demonstrates the utility of dynamic, quantitative and multi-scale techniques in understanding the different cellular processing routes of functionalised nanomaterials. This correlative approach has wide implications for assessing the biopersistence of MWNT aggregates elsewhere in the body, in particular their interaction with macrophages in the lung.

Keywords Biocompatibility; Carbon nanotube (CNT); Aggregation; Microglia; Brain

1. Introduction

Functionalised carbon nanotubes (CNTs), such as single-walled carbon nanotubes (SWNTs) and multi-walled carbon nanotubes (MWNTs), are receiving increasing attention as delivery vehicles for therapeutic and diagnostic agents [1-6]. Due to the ability of some CNTs to cross the blood-brain barrier (BBB) [7, 8], CNTs are being designed to target and deliver therapeutic molecules to neuronal cells in the brain. Dual functionalised acid oxidised Angiopep-2 modified polyethylene glycol (PEG-)MWNTs and, to a lesser extent, PEG-MWNTs, can target and cross the BBB *in vivo,* following intravenous injection in mice [8]. In neurotherapeutic applications, CNTs are also being developed as neural scaffolds, for example to drive neural regeneration across lesion sites [8-11]. CNT coatings on neuronal implants have been shown to improve electrical properties and decrease inflammatory responses [12]. Amine-modified SWNTs have served effectively as tissue scaffolds in neurological applications, limiting ischemic injury in rat stroke models [9]. Additionally, the

ability of certain CNTs to cross the BBB raises the risk that any CNTs present in the circulatory system due to accidental exposure may also access the brain. Due to these multiple routes of CNT exposure to the brain, it is necessary to assess and control cellular interactions with CNTs, and to understand their biopersistence and bioreactivity.

Of the cell types in the brain, microglial cells form the active innate immune defence in the central nervous system (CNS). As the innate inflammatory response is implicated in many CNS diseases, *e.g.* Alzheimer's disease and Parkinson's disease, the activation state of microglia is an important monitoring parameter during exposure to CNTs. Before CNTs can be used therapeutically or as diagnostic agents, there is a need to assess and control their cellular interactions, *i.e.* to determine: the ability of microglia to process and internalise CNTs; which organelles are targeted inside the cells; the inflammatory state of microglia; and to assess whether the CNTs are safe for human therapeutic use. While concerns have been raised about the neurotoxicity of carbon nanostructures [13], there are few reports on the interaction of CNTs with microglial cells. In this regard, Bardi *et al.* injected pluronic F-127-coated MWNT into the visual cortex of mice and observed no adverse toxicological effects at the cellular level [13]. In addition, MWNTs loaded with deoxyribonucleic acid (DNA) and small interfering ribonucleic acid (siRNA) also induced no significant changes in cell proliferation or inflammation and were internalised by a BV2 microglial cell line [14].

Variations in CNT physicochemical properties, such as length, aggregation state and changes in the surface chemistry/functionalisations of CNTs, will affect immune responses and could contribute substantial cytotoxicity within the time frame of CNT clearance [15-17]. For instance, Poland *et al.*[18] reported potentially asbestos-like inflammation, lesions and frustrated phagocytosis in mice exposed to long (>10 μm) CNTs, while shorter (5 μm) and bundled CNTs, more similar to the MWNTs used in the present study, did not elicit such a response. An increased density of functional groups or defectiveness of the CNTs may reduce

biopersistence, but may also increase cellular uptake and modulate immune or cytotoxic responses of the cells. The dispersion state of CNTs has been identified as one of the factors influencing cellular uptake and the profibrogenic macrophage responses to MWNTs [19]. In the lung, dispersed carboxylated MWNTs were more readily taken up by alveolar macrophage cells and induced more prominent TGF-β1 and IL-1β production both *in vivo* and *in vitro* compared to non-dispersed MWNTs [19]. Additionally, Al-Jamal *et al.* [20] have demonstrated differences in organ distribution and excretion of radiolabelled ammonium functionalised CNTs injected into mice which was attributed to differences in the degree of chemical functionalisation and hence CNT individualisation.

In the brain, MWNTs may be present in both dispersed and agglomerated states. MWNT clusters have been observed *in vivo* following cortical stereotactic administration into the mouse brain cortex [21], while it has been shown that CNT aggregates could become detached from implanted neural interfaces in rats [12]. CNTs designed as drug delivery vehicles could transcytose across the BBB as individual nanotubes or clusters. However, few studies to date have considered the cellular response to the *aggregated* CNT population. Sato *et al.* [22] analysed injected aggregates of oxidised MWNTs within murine subcutaneous tissue using high resolution transmission electron microscopy (TEM) and Raman spectroscopy. They observed large aggregates that were present in the intercellular space, which did not undergo degradation at time points measured up to two years after injection. By contrast, it was suggested that small aggregates were phagocytosed by macrophages, where they were gradually degraded within lysosomes [22]. While these results have important implications for the biopersistence and biocompatibility of MWNTs, the techniques used provide only snapshots in time of the distribution and structure of extra- and intra-cellular MWNT aggregates. Single time-point imaging provides limited information on dynamic uptake processes. For example, the small aggregates which are observed within

macrophage cells after two years may have been initially presented to cells as small aggregates, or alternatively they could have been broken/untangled from larger aggregates. Without stereological analysis of the time-dependence of aggregate sizes, which is difficult to achieve with the limited sampling inherent in TEM analysis and animal experiments, it is not possible to distinguish between these two scenarios. Dynamic techniques which are able to track the same extracellular MWNT aggregates over time would provide more information on the extracellular processing and internalisation processes controlling the ultimate biopersistance of these materials. For example, Jin *et al.*[23] have used the intrinsic band-gap fluorescence of SWNTs to track their interactions fibroblast cells, to provide evidence for SWNT exocytosis. However, this analysis was performed on individualised SWNTs only. Since a mixed population of individual and aggregated MWNTs will often be present in cell culture medium, a multi-scale/modal analysis is required to (a) monitor the uptake of both the aggregates and individual MWNTs at the cellular level and (b) correlate this analysis with higher-resolution, nano-scale imaging, in order to obtain insights into the extracellular processing and internalisation mechanisms. Furthermore, there are relatively few studies which quantify the amount of unlabelled MWNTs that come into contact with, or are internalised by, cells and which correlate this information to cell toxicity. Raman spectroscopy has been used to determine SWNT concentrations in washed macrophage cell samples [24] as well as in fibroblast cell lysates [25]; however, resonance effects make direct quantification challenging.

In this study, the hypothesis that the severity of the oxidative treatment controls the ability of phagocytic cells to break down and internalise aggregates of MWNTs is tested for the first time. A combination of light and scanning electron microscopy (SEM) was used to provide coupled dynamic and static information about the process by which phagocytic cells break up extracellular MWNT aggregates and provide information on whether the extracellular

aggregates are fully internalised by microglial cells. 3D SEM and TEM are used to track, at the subcellular level, how both the aggregates and individual MWNTs are processed and internalised, as well as their destination inside the cells. Cellular uptake of each format of MWNTs was quantified by UV-vis spectroscopy and correlated to inflammation, metabolism and activation of the microglial cells. Importantly, this study is performed without the use of fluorescently labelled probes, which could alter physicochemical properties and biological-interaction of MWCNTs. More generally, microglial cells are capable of macrophage-like activities, such as phagocytosis and antigen-presentation [26], and thus represents an important phagocytic cell model for studying the role of aggregation in the biopersistence of MWNTs.

2. Materials and Methods

2.1 Preparation and characterisation of MWNTs

Acid oxidation functionalisation. Pristine MWNTs were purchased from Arkema SA, France. In a typical reaction [27], 300 mg of Arkema MWNTs and 30 mL of concentrated sulphuric acid (A.R. grade, 98%, Sigma-Aldrich, UK) and nitric acid (puriss. p.a. plus, 65%, Fluka, UK), mixed at a volume ratio of 3:1 was heated to reflux at 120°C. After 30 minutes of heating, the reaction solution was cooled and then diluted with 500 mL of icy water. In order to remove the carbonaceous debris generated, a base wash process was carried out, as previously described [27]. The acid oxidized MWNTs (AO-MWNTs) were first washed with distilled water through a sintered glass filter, using a 0.45 μm polytetrafluoroethylene (PTFE) membrane, until the filtrate was colourless and the pH reached that of the distilled water (~ 5.5). Subsequently, the AO-MWNTs were washed with approximately 500 mL of 0.01 M sodium hydroxide (AnalaR grade, VWR, UK), until the brown dark colour filtrate ran clear. The base washing removes residual carbonaceous debris, reducing the confounding effects of

remnant carbonaceous debris for detecting the degradation process or the bioreactivity of the MWNTs [27-29]. The solution was washed once again with distilled water until the filtrate reached a neutral pH. Finally, the MWNTs were washed with approximately 500 mL of 0.01 mol/L HCl (AnalaR grade, BDH) and then washed to neutral pH once again. Acid:MWNT ratios (volume/mass, mL/mg) of 20 to 100 were used for MWNT shortening (referred to as 20AO and 100AO, respectively). AO-MWNTs prepared in this way are commonly used in the fields of environmental and occupational health, as they are well dispersed in aqueous media and, unlike MWNTs functionalised with positive charges, do not damage cellular membranes [30].

Raman spectroscopy. Raman spectra (1000-1800 cm^{-1}) were collected on a LabRam Infinity Raman spectrometer (Horiba, UK), using a 532 nm laser (scan time 90 s, an average of 3 scan cycles). The D/G intensity ratio was determined from the ratio of integrated areas under the Raman bands at around 1350 cm^{-1} (D-band) and 1580 cm^{-1} (G-band) [31]. Average values and standard deviations (SD) were obtained from five independent measurements.

Zeta potential measurements. MWCNTs were prepared as suspensions at a concentration of 10 μg/ml in sterile distilled water and in the culture medium used for cell exposure. The samples were briefly sonicated and vortexed before the zeta potential assessment using a Malvern Zeta NanoSizer (Malvern, UK).

UV–vis spectroscopy. The water compatibility of the MWNTs was characterized by UV-vis spectroscopy (Lambda 950, Perkin Elmer, UK). As-received and functionalised MWNTs were bath sonicated (45 kHz, 80W, VWR International, UK) in high-performance liquid chromatography (HPLC) water for 20 min with different initial powder loading concentrations of 100 μg/mL, 500 μg/mL, 1 mg/mL and 2 mg/mL. MWNT aggregates were then settled by centrifugation for 15 min at 10,000 g. The supernatant was carefully decanted

and the concentration of MWNTs determined by means of UV absorbance and application of the Beer-Lambert law, formulated as: $A = \varepsilon \cdot c \cdot d$, where A is the measured UV absorbance; ε is the extinction coefficient (35.10 mL·mg^{-1}·cm^{-1} for Arkema MWNTs at 800 nm [32]) and d is the light path length (cuvette length = 1 cm in this study). The AO-MWNTs showed significantly enhanced water compatibility compared to the pristine MWNTs [33].

SEM/filtration method. A membrane-filtering protocol was adapted from a previously published study by Müller *et al*. [34]. MWNT suspensions were prepared in complete medium (Dulbecco's Modified Eagle's Medium (DMEM)) supplemented with 5% foetal bovine serum (FBS, Sigma, UK), 8 mM L-glutamine (Sigma, UK), 100 U/L penicillin and 100 µg/mL streptomycin (Sigma, UK)) at a concentration of 10 µg/mL, and ultrasonicated for five min at room temperature (RT). After an additional 30 minutes settling time, 1 mL of suspension was passed through 3 µm membrane filters (13 mm diameter Isopore membrane plain, Millipore, UK) using a syringe and filter holders (Sartorius Stedim Biotech, Germany). Membranes were then rinsed with 1 mL deionized water (DIW) and dried at 60ºC for 60 min. Samples mounted on aluminium SEM stubs were gold-coated and imaged by SEM using a Zeiss Auriga FIB-SEM (Carl Zeiss NTS).

2.2 Exposure of N9 microglia to MWNTs

Cell culture. The immortalised microglial N9 cell line, produced through oncogenic retroviral transformation of embryonic day 13 mouse microglial cells [35], was used throughout this study. The N9 cell line has been used extensively in microglia reactivity studies and closely mimics the responses by primary microglia [36]. The N9 cells were maintained in complete medium at 37°C in 5% CO_2.

Microglial exposure. Microglia cells were seeded on 6, 24 or 48-well plates at a density of 4.5×10^4 cells/cm^2, by utilizing a haemocytometer to count cell numbers. The cells were

maintained in complete medium and cultured for 24 hrs prior to experimentation, to allow them to recover a resting phenotype. The MWNTs were prepared and handled in sterile conditions during experiments and stored in water at 4˚C. Before microglial exposure, the MWNT were diluted in complete medium and ultrasonicated for five min at RT. Supplementary information on the stability of MWNT in complete medium is available in Supplementary Fig. 2. Immediately after sonication, MWNT suspensions were exposed to the cells at the desired concentrations (1-10 μg/mL) for 24 hours. All experiments were performed in triplicate.

Endotoxin test. Before examining the cytotoxicity of the MWNTs, the endotoxin content of the samples was assessed. An endotoxin assay was performed using the *Limulus* Amebocyte Lysate (LAL) Chromogenic Endotoxin Quantitation Kit (Thermo Scientific, UK). The endotoxin content of pristine, 20AO and 100AO MWNTs was 0.004 ± 0.002, 0.84 ± 0.06 and 0.97 ± 0.12 EU/mL (mean ± SD), respectively, concentrations which did not cause microglial toxicity or activation (Supplementary Fig. 3).

2.3 Uptake of MWNTs by N9 microglia

Live-cell imaging. Real-time light microscopy imaging was performed on a Nikon TU2000 epifluorescence microscope (Nikon Instruments Inc., Melville, NY, USA) in a live imaging chamber at 37ºC and 5% CO_2. The N9 microglia were seeded on a 35 mm plastic bottom Ibidi dish (Thistle Scientific Ltd., UK) at a density of 2×10^5 and incubated overnight at 37^{o}C. The medium was replaced with complete medium containing 10 μg/mL of suspended pristine or 100 AO MWNT, and live cell imaging was initiated 30 min after first exposure. High resolution images were then acquired every four minutes using a 20× objective lens (Nikon) for 0.5-48 hours. Images were compiled into videos using ImageJ software (v.1.4, National Institutes of Health, Bethesda, MD, USA), with minimal loss of resolution. Each experiment

was conducted more than three times with similar results, and a representative video at each condition is presented as supplementary data (videos 1 and 2).

Correlative electron microscopy. For focussed ion beam scanning electron microscopy (FIB-SEM) experiments, the same cells imaged by live cell microscopy were fixed in 3% gluteraldehyde (Agar Scientific, UK), osmicated and dehydrated in a graded series of ethanol as for TEM preparations. Cells were then critical point dried using liquid carbon dioxide in a Tousimis Samdri 795 critical point dryer (Tousimis Research Corp., USA). Critical point dried samples were sputter coated with 10 nm gold for electrical conductivity before being imaged in a Zeiss Auriga FIB-SEM (Carl Zeiss NTS). The focussed ion beam was used to expose serial cross-sections within a cell and SEM images were acquired of the cell/MWNT interface using both secondary electron (SE) and backscattered electron (BSE) modes.

UV-vis spectroscopy. To quantify the amount of AO MWNT uptake by N9 microglia after 0, 2, 4, 6 and 24 hrs of exposure, the concentration of AO MWNTs remaining in cell medium after incubation with N9 microglia was measured using UV absorbance. Medium containing 100 or 20AO MWNTs was bath sonicated (45kHz, 80W, VWR International) for 20 min. The concentration of MWNTs was then determined by UV absorbance and application of the Beer-Lambert law as detailed above. The concentration and hence uptake of pristine MWNTs could not be quantified using this method due to the high degree of MWNT aggregation in the cell medium. Instead, pristine MWNT uptake was qualitatively assessed by live cell imaging and electron microscopy.

2.4 Determination of viability and inflammatory response

Lactate dehydrogenase release assay. Lactate dehydrogenase (LDH) release was used to quantify cellular membrane integrity as a parameter of cell viability. Microglia were grown in 24-well plates as described above. Following 24 hrs of CNT treatment, 10 μL of cell medium

were transferred to a 96-well plate and mixed with 100 μL of LDH reagent (Abcam, UK) to measure the levels of released (extracellular) LDH. The microglia were then lysed with the kit's cell-lysis solution (in the original incubation medium) and 10 μL of cell medium was transferred to a 96-well plate and mixed with 100 μL of LDH reagent to measure total (intracellular plus extracelluar) LDH. Optical density (at 450 nm) was measured after 5-10 mins following addition of LDH reagent, with cell viability quantified as the optical density ratio of released LDH to total LDH. The adenylyl cyclase inhibitor MDL-12330 (50 μM × 24 hrs) (Sigma, UK) was employed as a positive control for cell death.

Cell viability assay. The MTS (3-(4,5-dimethylthiazol-2-yl)-5-(3-carboxymethoxyphenyl)-2-(4-sulfophenyl)-2H-tetrazolium) assay was used to quantify metabolic activity as a second parameter of cell viability [37]. Microglia were grown in 96-well plates as described above. Following CNT treatment, microglia were washed with complete medium and incubated with fresh complete medium (100 μL) containing 10 μL MTS reagent (Sigma, UK). Microglia were incubated at 37^{o}C for 1-2 hrs and the optical density measured at 450 nm to determine intracellular NADH levels. Viability was determined from the optical density as a percentage of control cells. Similarly to LDH assays, the adenylyl cyclase inhibitor, MDL-12330, was employed as a positive control for cell death.

Nitric oxide quantification. Due to its short half-life, production of nitric oxide (NO) was assessed through quantification of its stable metabolite, nitrite (NO_2^-), using the Griess reaction [38]. Following 24 hrs of CNT treatment, 75 μL of cell culture medium was transferred to 96 well plates and incubated with 75 μL of Griess reagent (sulfonilamide plus 1-(naphthyl)ethylenediamine, Sigma-Aldrich, UK) at RT in the dark. Levels of nitrite were quantified by measuring absorbance at a wavelength of 540 nm after 5-10 min incubation. Optical density was converted to nitrite concentration using a sodium nitrite standard curve.

TNFα, IL-1β and IL-6 cytokine ELISA. The effect of MWNT exposure on the release of the pro-inflammatory cytokines tumour necrosis factor alpha (TNFα) and interleukin (IL)-1β and -6 by N9 microglial cells was assessed after a 24 hr CNT treatment by quantifying cytokine concentration in the cell culture medium by means of an Enzyme-Linked Immunosorbent Assay (ELISA, Peprotech, London, UK), in accordance with the manufacturer's instructions.

Reactive oxygen species quantification. Production of reactive oxygen species (ROS) was quantified with the use of 2'-7' dichlorofluorescin diacetate (DCFDA, Sigma-Aldrich, UK), a non-fluorescent, cell permeable probe which becomes highly fluorescent upon oxidation by ROS. Briefly, N9 microglia were seeded in dark-walled, clear, flat-bottomed 96-well plates. Following 24 hrs of CNT treatment, the medium was removed and replaced with fresh medium containing 25 μM DCFDA. As a positive ROS production control, microglia were treated with 50 μM tert-butyl hydrogen peroxide (Sigma-Aldrich, UK) for 4 hrs prior to incubation with 25 μM DCFDA. Following addition of DCFDA, the microglia were incubated at 37^{o}C for 45 mins, during which time they were protected from light. The fluorescence was then measured with a plate reader set at λ_{ex} = 485 nm and λ_{emm} = 535 nm.

Cell proliferation assay. Microglial proliferation was measured by quantifying live microglia with the use of Trypan blue dye, which is internalized into cells with compromised membranes (*i.e*. dead/damaged cells) and excluded from cells with intact membranes (*i.e*. live/healthy cells). Briefly, N9 microglia that had been plated in 6-well plates were treated with CNT. Following 72 hrs of incubation, the cell medium was replaced with fresh medium (1 mL) and the microglia were thoroughly scraped from the well. A total of 10 μL of medium was then mixed with 10 μL of Trypan blue and placed on a haemocytometer to count the

number of live microglia in a 0.1 μL volume. The counting procedure was repeated twice for each condition.

2.5 Determination of intracellular fate of MWNTs

TEM. For TEM imaging and analysis, N9 microglia were seeded on 6-well plates and exposed to 10 μg/mL of MWNTs for a pulse of two hours, followed by chase periods of 2, 24 and 72 hrs in the absence of MWNTs. After the chase period, N9 microglia were washed, fixed in 2.5% gluteraldehyde in 0.1M PIPES buffer (pH 7.2) for 1 hr at 4°C, then washed twice in deionized water. Samples were post-fixed with 1% osmium tetroxide (Sigma-Aldrich, UK), before being dehydrated in a graded series of ethanol, washed twice in dry acetonitrile and then infiltrated with a mixture of 50% acetonitrile and 50% Quetol 651 resin mixture (Agar Scientific, UK) for 24 hrs [39], followed by 4 daily changes of the Quetol resin mixture. The resin was then cured at 60°C for 24 hrs. Ultrathin sections, 60-90 nm thick, were cut using a Leica Ultracut ultramicrotome (Leica, UK), with a 35^{o} wedge-angle diamond knife and collected on 300 mesh bare copper grids in distilled water.

Multiple sections (>100 cells) from 3 exposures from cultured cells were viewed in a Titan 80-300 scanning/transmission electron microscope (S/TEM) (FEI, UK). Bright-field TEM (BF-TEM) and high-resolution TEM (HR-TEM) images were captured on a US1000 2k×2k CCD camera (Gatan, UK). The accelerating voltage used in this study was 80 kV, which is below the threshold energy for knock-on damage in MWNTs [40]. In order to confirm that no significant damage to the MWNTs occurred under the electron beam, time course beam damage studies were conducted. No visible damage to MWNTs was observed by HRTEM after direct exposure to the beam for 60 mins.

Statistical analysis. Data are expressed as mean $\pm$ standard error of the mean for three independent experiments measured in triplicate, unless stated otherwise. Statistical

significance was assessed by means of a one-way ANOVA with a Tukey's *post-hoc* test, with statistical significance which was deemed at $p < 0.05$.

3. Results

3.1 MWNT characterisation

Pristine and AO MWNTs were characterized by SEM and high resolution TEM (Fig. 1a-i) to verify their purity and crystalline structure. Increasing the acid:MWNT ratio (volume/mass, mL/mg) from 20 to 100 decreased the MWNT length distribution from 0.32 ± 0.30 μm (Fig. 1d,e) to 0.19 ± 0.21μm (Fig. 1g, h) [41]. The outer walls of the MWNTs were significantly damaged by the acid oxidation treatment, and features such as thinning of MWNTs and delamination were observed in agreement with previous reports [33] (white arrows in Fig. 1f, i). Comparatively little amorphous material (black arrows) was observed on MWNT surfaces by HRTEM, suggesting that oxidation debris generated by acid treatment was adequately removed by base-washing (Fig. 1f, i).

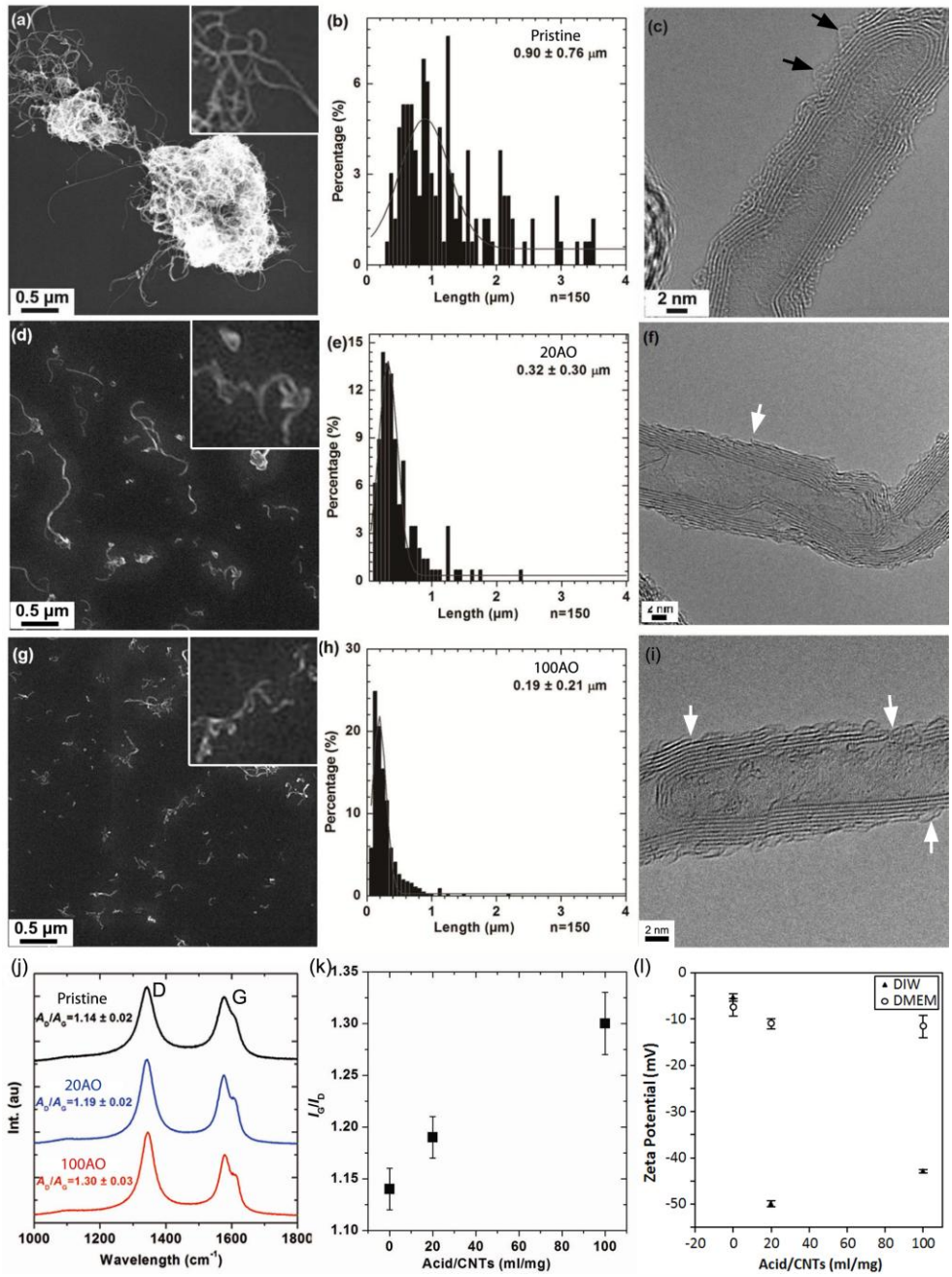

Figure 1. Characterisation of pristine and AO MWNTs. (a, d, g) SEM images and (b, e, h) corresponding length distributions of pristine, 20AO and 100AO MWNTs, respectively. (c, f, i) High resolution TEM micrographs show MWNT structure and defects in the graphitic walls (white arrows) and the presence of a small amount of amorphous material on the CNT surface (black arrows). (j, k) Raman spectra showing increasing D:G ratio with increasing degree of oxidation. (k) Zeta potentials of MWNTs measured in deionised water and 5% FBS supplemented DMEM.

The main features in the Raman spectra of MWNTs were the two peaks at around 1580 cm^{-1} showing the graphite band (G-band) and at around 1350 cm^{-1}, the defect band (D-band) (Fig. 1j). The G-band is associated with the in-plane vibrations within (intact) graphene layers of the MWNTs walls, while the defect band (D-band) is attributed to disorder in the graphene structure, carbon vacancies, functional groups, graphene layer edges or amorphous carbon content. Therefore, the relative peak intensity ratio of the D- and the G-band gives an indication of the defect density of the MWNTs [42]. Raman spectroscopy measurements indicated an increase in disorder of CNTs framework with increasing acid:MWNT ratio as reported previously [41] (Fig. 1j). Thermogravimetric analysis (TGA) and X-ray photoemission spectroscopy (XPS) provided complementary evidence that increasing the severity of the acid oxidation treatment led to an increase in the density of both defects and oxygen-containing functional groups (Supplementary Fig. 1).

AO MWNTs showed significantly enhanced water compatibility compared to the pristine MWNTs, as indicated by large zeta potentials and the dark colour of the supernatant solutions after centrifugation (10,000 g, 15 mins). The zeta potential of the 20AO and 100AO MWNTs decreased in the FBS supplemented cell culture media compared to water (Fig. 1k), which is significant as this increases the propensity of AO MWNTs to form aggregates within the medium. Interestingly, Heister *et al*. [43] reported a similarly reduced stability of oxidised SWNTs in cell media compared to water, and attributed this result to the competing effects of salt concentration (which decreases the stability of the SWNT dispersion) and adsorption of serum proteins, which, in turn, increases stability. Light microscopy of MWNT aggregates in complete medium was used to measure aggregate sizes of ~100 aggregates that had diameters larger than 2.25 μm (Supplementary Fig. 4). Pristine, 20AO and 100AO MWNT aggregates displayed similar mean aggregate diameters of 7 ± 7 μm, 8 ± 6 μm and 5 ± 4 μm, respectively. SEM micrographs of MWNT aggregates retained on membrane filters

(Supplementary Fig. 4) confirmed the similarities in aggregate diameters between MWNTs with different degrees of oxidation.

3.2 Live imaging of cellular internalisation of extracellular MWNT aggregates

Viewed under the optical microscope, opaque black particles 1–20 μm in diameter were visible in cell culture media containing pristine or AO MWNTs (Fig. 2a,g). These particles were confirmed by subsequent SEM imaging to comprise of large aggregates of MWNTs (Fig. 3). While pristine MWNT aggregation is expected, AO MWNT aggregation can be explained by the reduced zeta potential of the AO MWNTs in the 5% FBS supplemented DMEM cell culture media compared to DIW.

When N9 microglia were incubated with the 100AO MWNTs (Supplementary Video 1), cells which came into contact with aggregates of 100AO MWNTs often remained in close proximity to the aggregate. The interaction between the plasma membrane and aggregate was strong enough that once attached to a cell, a previously stationary MWNT aggregate could be 'pulled' tens of microns across the plate. These interactions were initiated during the first 1-3 hrs of incubation (Fig. 2a, b), and 100 AO MWNT aggregates appeared to be fully surrounded by microglial cells after 12 hrs of exposure (Fig. 2c). By ~48 hours, the original aggregate size (20 μm) was reduced while smaller opaque particles less than 10 μm in diameter were often observed in the surrounding microglia (Fig. 2e, arrows). These observations are consistent with the smaller aggregates of 100AO MWNTs having been broken off from the original large aggregate by the cellular activity.

The microglia which had been observed by live cell imaging, were subsequently prepared for SEM analysis by critical point drying (Fig. 3). Opaque particles observed by light microscopy

were confirmed to be MWNT aggregates by SEM imaging, and N9 microglia were observed to be interacting with the 100AO MWNT aggregates (Fig. 3a,b). Microglia were sectioned using the focused ion beam, and SEM imaging of serial cross-sections revealed the presence of sub-micron aggregates ~400 nm in diameter (Fig 3c, d, white arrows) which had been completely internalized by the microglia. Thus, correlative live imaging and FIB-SEM support the interpretation that interactions between microglia and AO MWNTs lead to the break-up of aggregates and subsequently their internalisation by cells (Fig. 3).

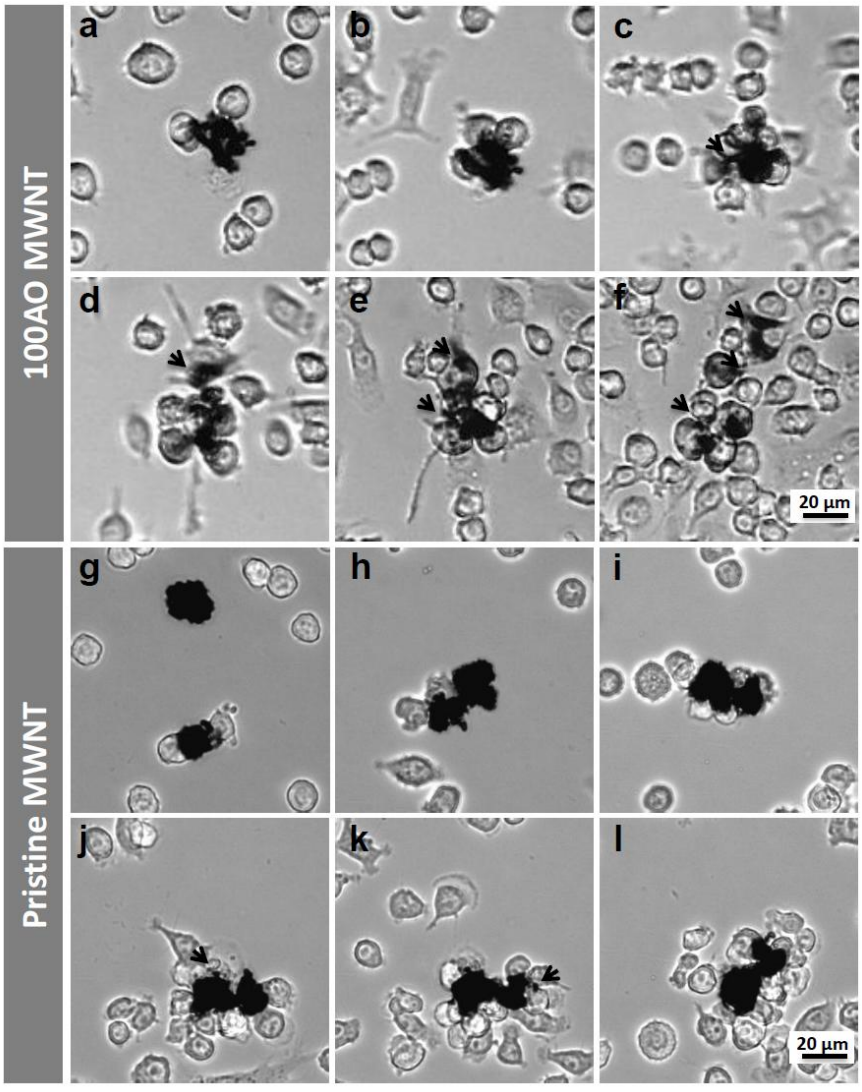

Figure 2. Selected light micrographs from live cell imaging videos of N9 microglia exposed to (a-f) 100AO and (g-l) pristine MWNTs for 48 hours (see also supplementary video 2).

Images here are acquired (a,g) 1 hour (b,h) 3 hours (c,i) 12 hours (d,j) 30 hours (e,k) 40 hours and (f,l) 48 hours after exposure. Irregular opaque particles ~20 μm in diameter are identified as MWNT aggregates. N9 microglia surround 100AO MWNT aggregates about 12 hours after exposure (c). Small aggregates (<10 μm in diameter) were broken up from the main aggregate continually (c-f, marked with black arrows). Microglia are observed to surround pristine MWNT aggregates at ~30 hours (j). The majority of pristine MWNT aggregates remain intact after 48 hours, although some small aggregates (<4 μm in diameter) appear to have been broken away from the main aggregate (black arrows, j,k).

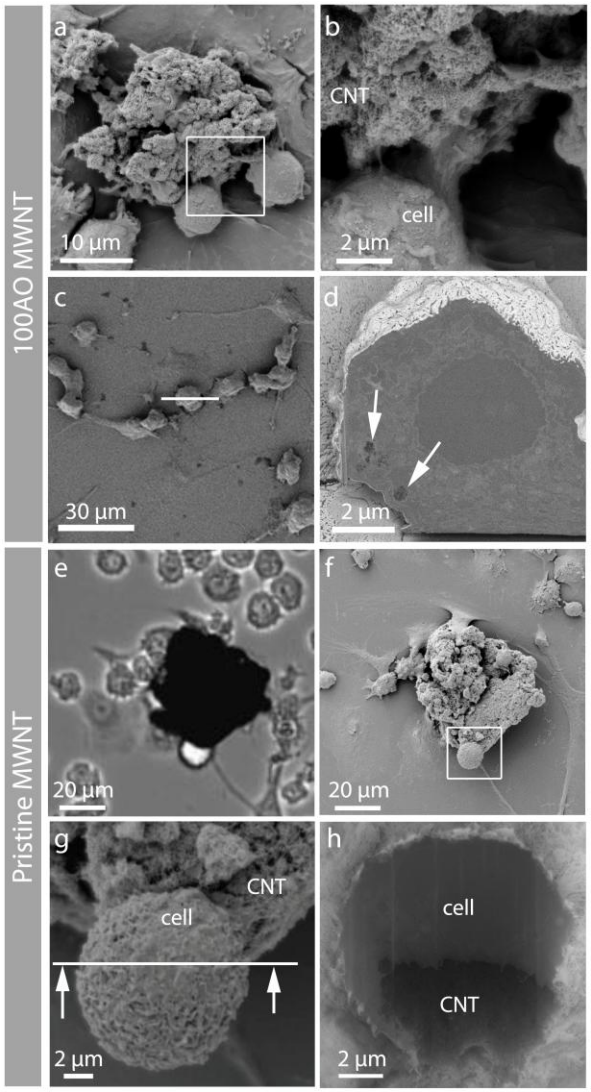

Figure 3. Correlative microscopy showing the interaction between 100AO and pristine MWNT aggregates and N9 microglia. (a,b) Low and high magnification SEM micrographs

showing N9 microglia interacting with an 100AO MWNT aggregate. (c) Top view of another N9 microglia, which was sectioned by FIB milling at the white line. (d) Back scattered electron (BSE) image of the cross-sectioned surface reveals the presence of sub-micron aggregates of 100AO MWNT inside the microglia (arrows). (e) Light micrograph of pristine MWNT aggregate and (f) corresponding SEM images of the same area after critical point drying at low (g) and higher (h) magnification. The partial wrapping of the microglia around part of the aggregate demonstrates the clearance challenge that large pristine MWNT aggregates presents to the cells.

Whilst extracellular aggregates of 100AO were found to be broken up by microglia and subsequently internalized, different behavior was observed in live-cell imaging of microglia incubated with pristine MWNTs. Microglia attached to pristine MWNT aggregates during the first 1-3 hrs and surrounded the aggregates after ~10 hrs (Fig. 2f-h, Supplementary Video 2). The majority of pristine MWNT aggregates remained intact after 48 hrs and microglia were found in close association with the surface of large extracellular aggregates (Fig. 3e-h). However, a small number of aggregates with diameters of less than 4 μm were observed after 30 hrs of incubation (black arrows, Fig. 2j, k) and N9 microglia were observed to engulf these small aggregates. Further SEM analysis demonstrated a close association of the microglia at the surface of pristine MWNT aggregates (Fig 3e-h), with microglia partially wrapped around the pristine MWNT aggregate which remained intact (Fig. 3h).

3.3 UV-vis quantification of AO MWNT uptake

After establishing that aggregates of AO MWNTs could be internalized by microglia, the ability to control the extent of internalisation by varying the D:G ratio (along with the associated small variations in CNT length) was determined. Pristine MWNT uptake was not evaluated using this method as the highly aggregated pristine MWNTs could not be re-

suspended in cell medium to a high enough degree to enable reproducible concentration measurements by UV-vis spectroscopy. Figure 4 shows the percentage of 100AO and 20AO MWNTs that was recovered in the cell medium after incubation with N9 microglia for various lengths of time. This measurement indirectly quantifies MWNT uptake and adhesion to the microglia, as the remaining MWNT fractions are most likely internalized by N9 microglia, or are associated with the plasma membrane tightly enough to not be readily washed off. Very little MWNT uptake and association is observed between 2 and 6 hrs. However, after 24 hrs of incubation, 52% ± 2% of 100AO MWNTs and 40% ± 3% of 20AO MWNTs were found to be interacting with N9 microglia.

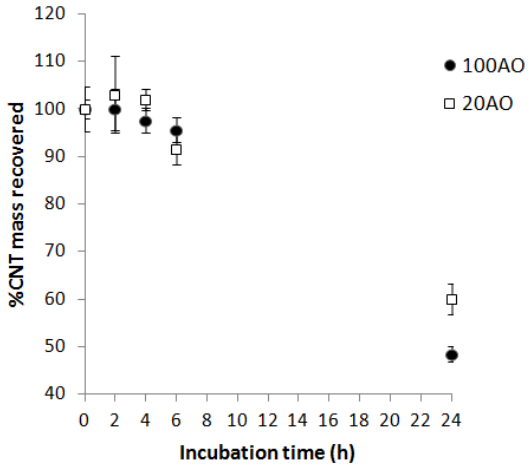

Figure 4. Concentration of 100AO and 20AO MWNTs remaining in cell medium after incubation with N9 microglia for varying times, quantified by UV absorption at 800 nm. The rest of the MWNTs are likely to have been internalised by N9 microglia or are strongly interacting with the plasma membrane.

3.4 Cell reactivity – toxicity, cytokine production and activation

Neither the pristine nor acid oxidized (20AO or 100AO) MWNTs had significant effects on the viability of microglia as measured by the MTS and the LDH release assays (Fig. 5a-h) at 24 hrs, up to a concentration of 20 μg/mL (pristine) or 10 μg/mL (AO). As a positive control,

N9 microglia were treated with the adenylyl cyclase inhibitor, MDL-12330 (24hrs, 100 μM), which resulted in a significant increase in LDH release (Fig. 5d) and a significant decrease in metabolic activity (Fig. 5h). Similarly, treatment with pristine or 20/100 AO MWNT failed to increase NO production (Fig. 5i-k) and also failed to induce release of pro-inflammatory cytokines (Fig. 5m-t), while treatment with LPS (500 ng/mL) as a positive control resulted in robust increase in NO production (Fig. 5l) and pro-inflammatory cytokine release (Fig. 5p, u). After incubation for 24 hrs with the MWNTs, only the pristine MWNT induced a significant increase in ROS activity in the microglia (Fig. 5v). 2.5, 5 and 10 μg/mL of MWNTs induced 1.6, 1.8 and 2.8 fold increases in ROS respectively, compared to controls. At the highest MWNT concentration (10 μg/mL), ROS activity was 25.7% of the maximal positive control induced by 50 μM tert-butyl hydrogen peroxide. In order to determine the longer term effects of MWNT exposure, cell proliferation was assessed after low concentrations (2.5 μg/mL) of MWNTs were incubated with microglia. No significant effect on cell proliferation was observed after 72 hrs of exposure to pristine, 20AO nor 100AO MWNTs (Fig. 5w).

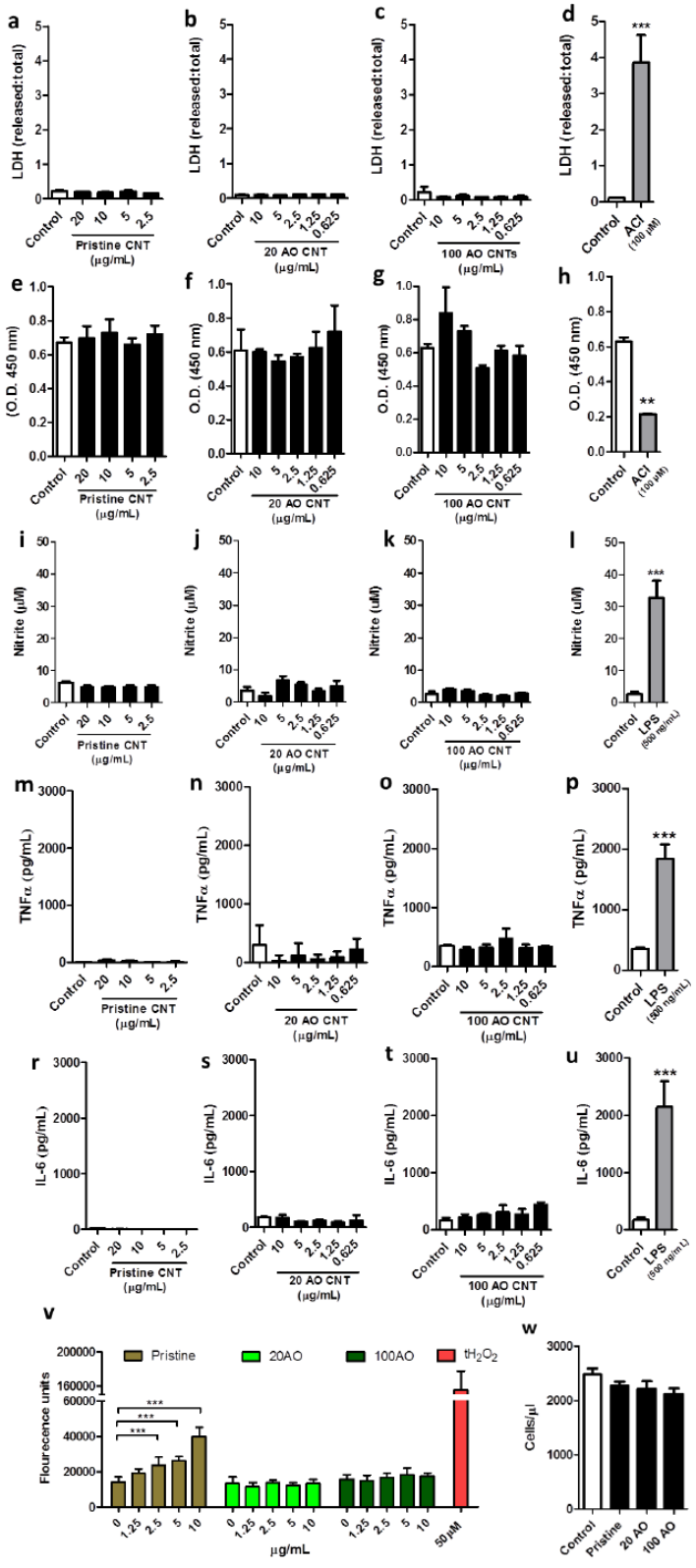

Figure 5. Microglial viability and inflammatory response after exposure to pristine or acid oxidized MWNTs. N9 microglia were treated with pristine, 20 or 100AO MWNT for 24hrs, after which time-point cell viability was measured through assessment of membrane integrity

through an LDH release assay (a-d) and metabolic activity through an MTS assay (e-h). Microglia were treated with an adenylyl cyclase inhibitor as a positive control for cell death (d, h). In addition, microglial reactivity was measured after a similar treatment by quantification of nitrite production through a Griess assay (i-l), release of pro-inflammatory cytokines TNFα (m-p) and IL-6 (r-u) through an ELISA, and quantification of ROS production (v). As a positive control, microglia were treated with lipopolysaccharide (LPS) (l, p, u) or with tert-butyl hydrogen peroxide (v). Microglial proliferation following 72 hrs of MWNT treatment was assessed through cell counting of trypan blue-excluding cells (w). Results are displayed as mean ± standard error of the mean of three independent experiments. **, *** denote $p < 0.01$, 0.005, respectively *vs.* control as determined by an unpaired Student's *t*-test (d, h, l, p, u) or a one-way analysis of variance (ANOVA), followed by a Tukey's *post-hoc* test.

3.5 TEM of intracellular MWNTs

The aim of TEM imaging was to study the intracellular processing of the MWNTs after known periods of time within the N9 microglia. Therefore, a pulse chase experiment was conducted in which cells were exposed to MWNTs for two hrs (pulse), after which any unbound MWNTs were removed by washing. After a further two hrs of incubation (chase), cells revealed similar distributions of 20AO and 100AO MWNTs. As no significant differences were observed between 100AO and 20AO MWNT distributions, TEM results from both oxidized MWNTs will be discussed together in this section.

AO MWNTs were observed at the plasma membrane of N9 microglia, and some MWNTs appeared to be inserted *into* the plasma membrane (Fig. 6b and 7a). AO MWNTs were also present as aggregates inside large (0.5-5 μm, Fig. 7b,d) and smaller (~400 nm) endosomes (Fig. 6c, 7c). Individual AO MWNTs were observed within the cell cytoplasm (Fig. 7b),

which could either indicate translocation of AO MWNTs across the plasma membrane, or escape from endosomal compartments.

After a 2 hr pulse, followed by a 24 or 72 hr chase, both types of AO MWNT were observed in the cytoplasm of N9 microglia, and also clustered within vesicles. After the 72 hr chase, AO MWNTs were additionally observed in multilaminar bodies, with concentric membrane structures and outer diameters of ~400-800 nm (Fig. 6i, 7i). In order to determine if the multilaminar bodies were related to autophagosomes, the expression of autophagy-related genes was investigated using quantitative reverse transcription polymerase chain reaction (qRT-PCR) [44]. However, no significant changes in the expression of genes normally associated with the induction of autophagy (ATG-5, ATG-7, ATG-10, ATG-12, ULK and BECN-1) were observed compared to controls (Supplementary Fig. 5). No AO-MWNTs were observed inside nuclei or mitochondria at any time-point, with these cell compartments appearing normal. High-resolution images of AO MWNTs found in the microglia cytoplasm after 24 hrs showed that the AO MWNTs were at varied stages of structural breakdown (Fig. 8). Morphological damage to the AO MWNT structure was observed, including highly disordered graphitic structures (Fig. 8a-c), and delamination of the outer walls of the AO MWNTs (Fig. 8d-f). However, the amount of structural disorder which can be attributed to intracellular degradation was not quantified, owing to a large range in the degree of MWNT defectiveness caused by the acid oxidation process itself [33].

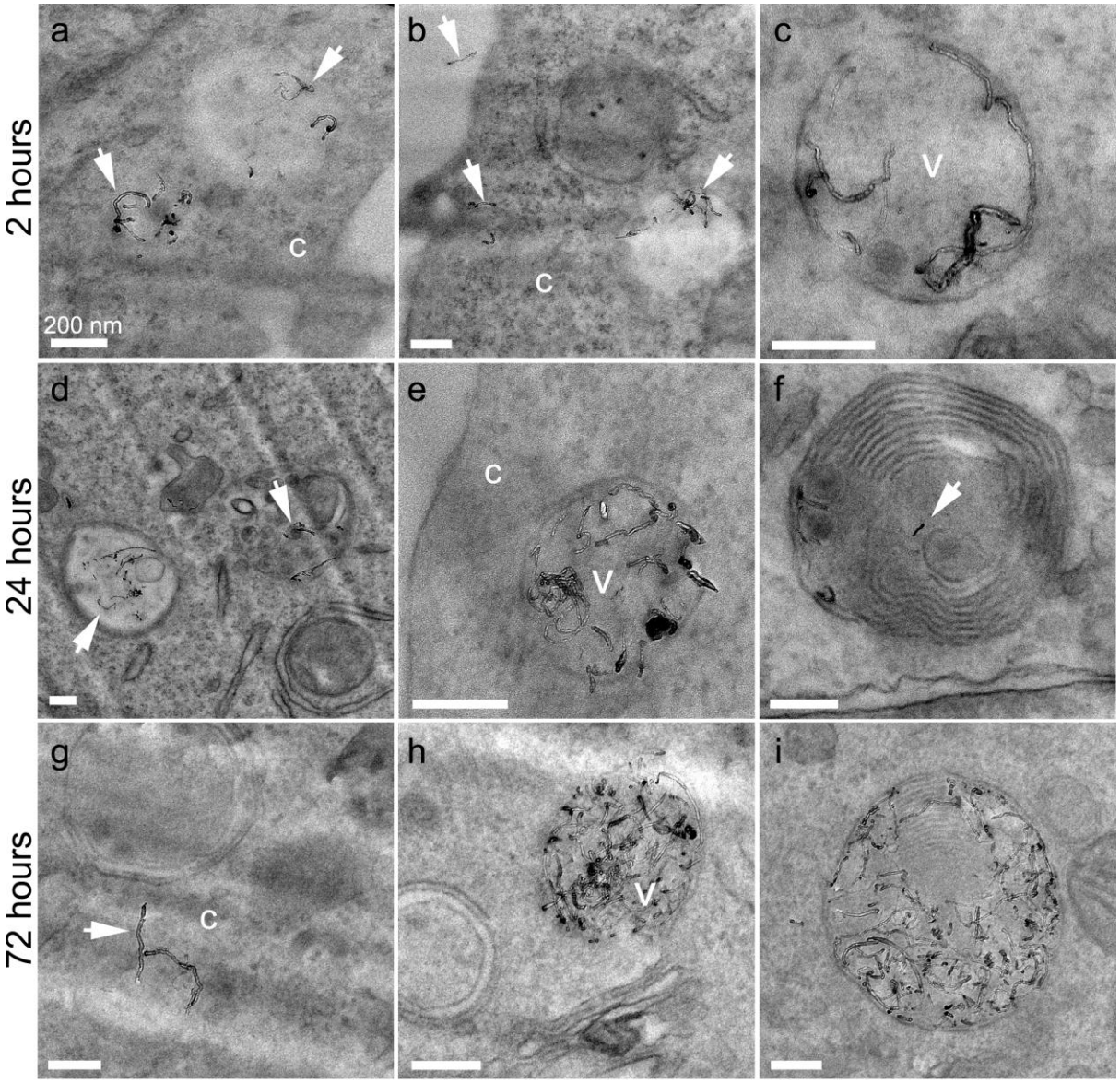

Figure 6. TEM micrographs showing 20AO MWNTs internalized by N9 microglia after 2 (a-c), 24 (d-f) and 72 (g-i) hrs. Selected MWNTs are marked with white arrows, and can be observed individually and in small clusters within vesicles (v) as well as in the cell cytoplasm (c). At longer time-points, multilaminar bodies are also observed containing MWNTs (f, i). All scale bars 200 nm.

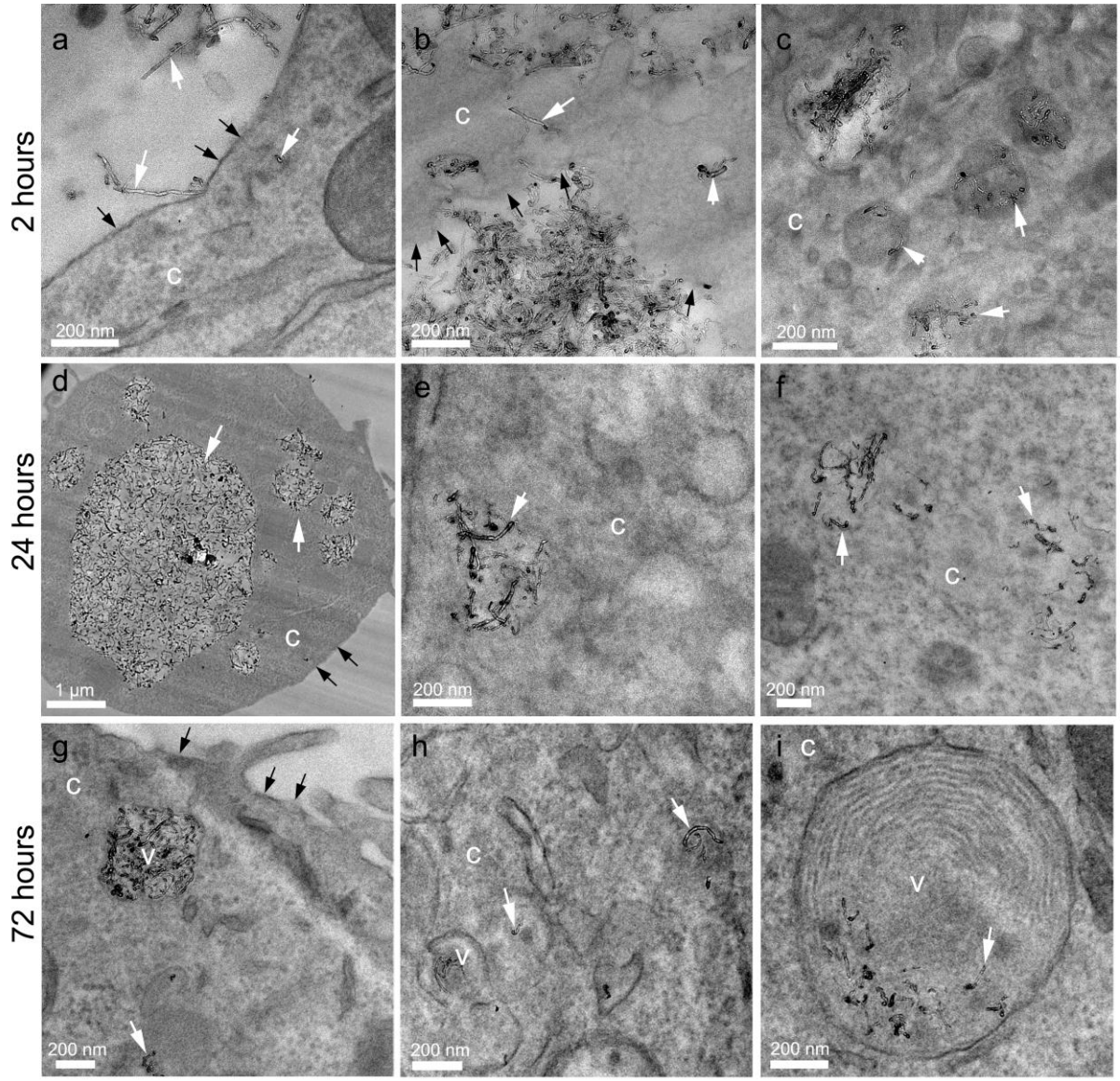

Figure 7. TEM micrographs showing 100AO MWNTs internalized by N9 microglia after 2 (a-c), 24 (d-f) and 72 (g-i) hrs. MWNTs (white arrows) are observed piercing the plasma membrane (black arrows), and are located within vesicles (v), the cytoplasm (c), and multilaminar bodies (i).

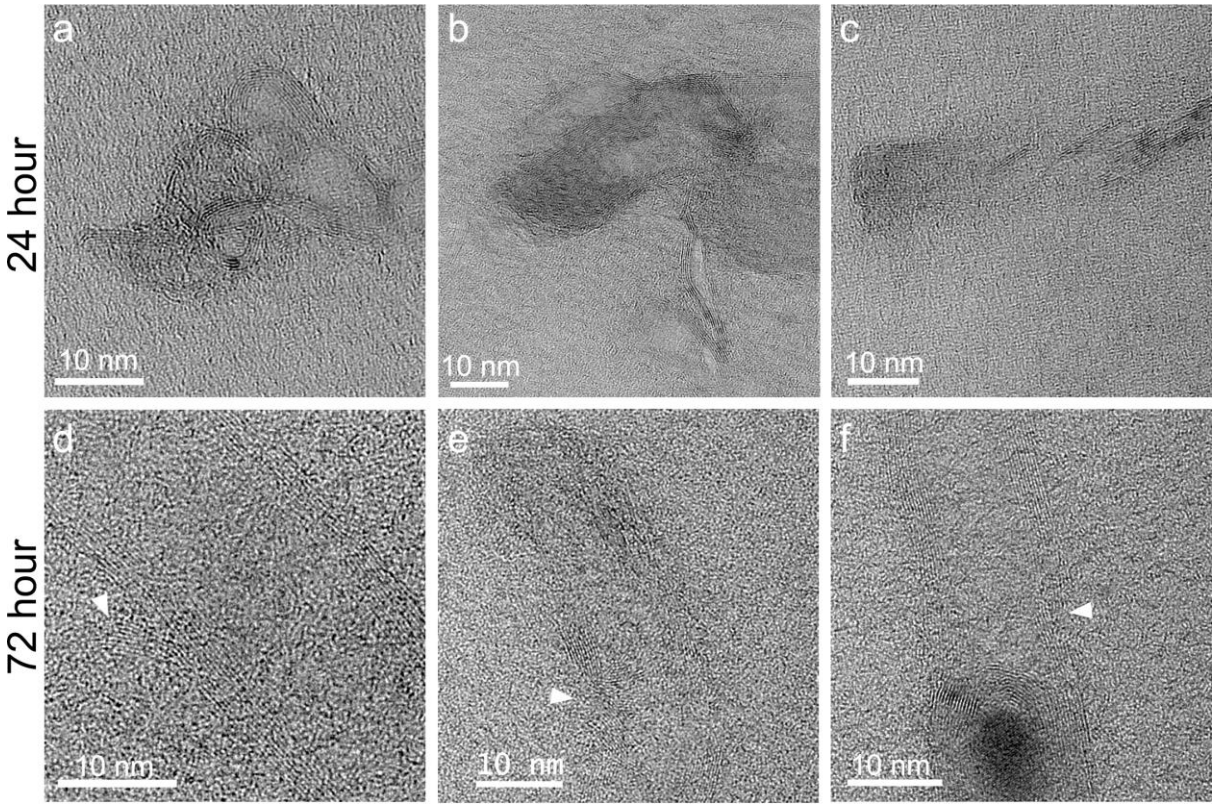

Figure 8. High-resolution TEM micrographs of individual 100AO MWNTs located within N9 microglia 24 and 72 hrs after exposure. Defective structures including kinks, bends and delamination of graphitic walls (arrows) can be observed at both time-points. Similar defects are observed in 20AO MWNT samples after 24 and 72 hour exposures to N9 microglia (not shown).

In contrast to AO MWNTs which were observed both individually and in clusters, and which were readily internalized by N9 microglia, TEM imaging showed that pristine MWNTs were mostly present within large micron-sized aggregates (Fig. 9). At all time-points, p-MWNT aggregates were observed in close association with the plasma membranes of cells and within large vesicles inside the microglia. Even after a 72 hr chase, some aggregates remained incompletely internalized by the microglia (Fig. 9c). This result agrees well with optical and SEM microcopy reported here (see Fig. 2g-l, 3h). In contrast to 20AO and 100AO MWNTs,

highly defective graphitic structures were not observed in pristine MWNTs. However, very few internalised p-MWNTs could be studied due to the limited uptake of these MWNTs.

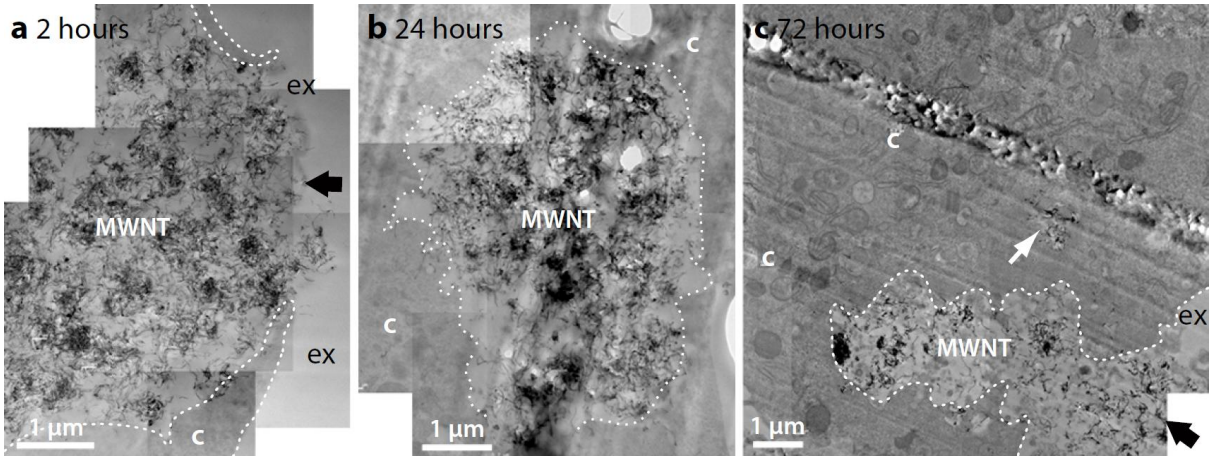

Figure 9. TEM micrographs of N9 microglia exposed to pristine MWNT (10 µg/mL) after (a) 2 hour-, (b) 24 hour- and (c) 72 hour chase. Pristine MWNTs are present as large aggregates (labelled MWNT) and are often incompletely internalised by N9 microglia (black arrows), even after 72 hours. Cellular membranes are indicated with white dotted lines to more clearly distinguish the cytoplasm (c) from the extracellular space (ex). An internalised aggregate of pristine MWNTs is indicated by the white arrow.

4. Discussion

C_{60} and SWNTs and MWNTs (pristine and functionalised) are known to be taken up into the brain, either *via* olfactory neurons or *via* the blood brain barrier, which has made the neurotoxicity of carbon nanostructures a pertinent issue [7, 8, 45, 46]. Here for the first time, the effects of pristine and AO MWNT exposure to microglia have been assessed using a correlative approach to analyze cellular interactions with extracellular and internalized multi-walled nanotubes and aggregates. Aggregation state has been identified as one of the factors influencing the cytotoxicity of MWNTs [47] and concerns exist about the potential for

MWNT clusters of particular sizes and aspect ratios to cause frustrated phagocytosis, leading to inflammation and possibly fibrosis [19]. Extracellular aggregates of MWNTs, which may be present in the brain following cortical stereotactic administration [21], detachment from implanted neural interfaces [12], or aggregation of individual CNTs which have crossed the BBB, were studied using light microscopy and correlative FIB-SEM. The use of this correlative approach has enabled the same internalisation events tracked by live cell imaging to be studied at higher resolution in the SEM, confirming the identity of the opaque particles as MWNT aggregates and providing evidence of AO MWNT internalisation as well as the close association of N9 microglia with the surface of both pristine and AO MWNT aggregates (Fig 3). The avoidance of any tagging procedures, and their associated changes to the CNT physiochemical properties, is a major advantage of this correlative approach.

Of major importance is the finding that extracellular aggregates of AO MWNTs can be broken down by phagocytic microglia without inducing changes in the cell metabolism/activation state. The exact mechanism of extracellular breakdown of 100AO MWNT aggregates by N9 microglia is not known, although we hypothesize that attachment of multiple microglia to a single aggregate may play role in the breakup of the aggregate through a disentanglement mechanism. The reasoning behind this hypothesis is as follows:

1. A single macrophage cell, a related phagocytic cell type, has been reported to generate forces of up to 8×10^4 pN on a pipette tip around 6-10 μm in diameter [48].
2. The critical force required to break an individual MWNT is reported to range from ~5×10^5 pN [49] to ~2×10^7 pN [50]. These values are at least an order of magnitude larger than the force exerted by a single phagocytic cell. Even accounting for the vacancies and related defects which are expected to be present in the walls of oxidized CNTs, molecular dynamical simulations suggest that this critical force is only reduced by a factor of two [51]. Breakage of individual MWNTs is therefore unlikely to be a

common occurrence during the extracellular processing of both pristine and AO MWNT aggregates by phagocytic cells.

3. In contrast, Blighe *et al*. found that the average force required to separate a junction between two SWCNT bundles within a nanotube film is only ~100 pN [52]. Also of relevance is their observation that the mechanical properties of the films had a strong dependence on the film morphology, and a comparatively weak dependence on the functionalisation of the constituent SWNTs.

While the separation force has only been estimated for SWNT bundles, if we assume similar separation forces between two individual MWNTs, these figures suggest that phagocytic microglia may be capable of MWNT disentanglement where fewer than ~100 junctions are required to be separated. In contrast, clusters of pristine MWNTs were rarely broken down by the microglia. Previous studies have demonstrated the importance of electrostatic interactions between CNTs and cell membranes during alternative uptake routes such as membrane piercing [53, 54]. Electrostatic considerations may also be important in the disentanglement process, however as the pristine and AO MWNTs used in the present study display similar zeta potential values in cell medium, the difference in disentanglement is likely dominated by other factors. Instead, the ability of microglia to break apart AO MWNT aggregates but not pristine MWNT aggregates may be related to the different *length*s of pristine and AO MWNTs, and therefore differences in the degree of entanglement , or number of contacts per nanotube, within the aggregate structure. Further work is required to determine the nanostructure within CNT aggregates, however performing this characterisation within the appropriate liquid environments presents a significant analytical challenge.

This work complements the work on CNT biopersistence by Sato *et al*. [22]. The disentanglement of aggregates of AO MWNTs could reduce the risk of fibrosis and increases the potential for internalisation, and therefore further intracellular biodegradation. The

finding that extracellular aggregates of AO-MWNTs, but not pristine MWNTs, can be broken down by microglia highlights the urgent need for future work to monitor whether extracellular aggregates can be broken down in other organs also, especially in the lung, and to determine which MWNT properties control this process. Studies using alveolar macrophages are currently under investigation in our laboratories.

Standard measures of dose (weight/unit volume of cell culture medium) used in toxicology testing do not measure the amount of material that comes in contact with the cells. Quantification of the amount of uptake of carbon nanomaterials is a great challenge and is essential for quantitative toxicology. While the spatial resolution of light microscopy allowed only aggregates of MWNTs to be qualitatively assessed during internalisation, the addition of UV spectroscopy provides a *quantitative* measure of the proportion of AO MWNTs internalized or adhered to the microglia. In contrast to the limitations of light microscopy, UV spectroscopy measurements are sensitive to both the individualized AO MWNTs and the loose agglomerates which may still be present in the recovered cell medium after bath sonication, and so provide a measure of the total AO MWNT population. Only a small percentage of AO MWNT internalisation was detected after 2-6 hrs of incubation (Fig. 4), which contrasts with the kinetics of SWNT internalisation by fibroblasts as measured by Holt *et al*. [25]. The Raman spectroscopy study by Holt *et al.* found that internalisation of dispersed SWNTs by endocytosis reached a steady state after one minute, and remained constant during the subsequent 48 hrs of continuous exposure [25]. The relatively slow uptake of AO MWNTs found here could be related to the disaggregation process detected earlier by live cell imaging, in which evidence of break-up of larger AO MWNT aggregates is only observed after ~12 hours (Fig. 2c). AO MWNTs were found to be readily internalized by microglia after 24 hours, with 52% ± 2% of 100AO MWNTs and 40% ± 3% of 20AO MWNTs interacting with N9 microglia after 24 hrs. This corresponds to a mass of

approximately 3.0 pg (2.6 pg) of 100AO (20AO) MWNT per cell. Despite the relatively high loading of AO MWNTs, as well as the continued presence of a significant fraction of extracellular MWNT aggregates after 24 hrs, 20/100AO MWNTs failed to cause any acute deleterious effects on cell viability, proliferation and inflammation at 24 hrs and failed to alter cell proliferation at the 72 hrs exposure time-point.

Using an sp^2 carbon-carbon bond length of 1.421 Å, MWNT diameter of 12 nm [33], and the nanotube lengths measured earlier, the mean mass of a MWNT containing ten walls is calculated to be 4.1×10^{-17} g for a 100AO MWNT and 6.9×10^{-17} g for a (longer) 20AO MWNT. Therefore, the estimated mean number of MWNTs per cell is 75000 and 40000 for 100AO and 20AO MWNTs, respectively. Despite the differences in the *number* of MWNTs taken up by (or adhered to) cells, this corresponds to similar AO MWNT *volumes,* approximately 0.1% of a microglial cell volume in both cases, assuming a spherical microglial cell 14 μm in diameter. The AO MWNT loadings reported in this work are lower than the ~0.6 vol% loading of protein-wrapped SWNTs within macrophage cells found by Bertulli *et al.* [24] using Raman spectroscopy for uptake quantification. Increased uptake of protein-SWNTs will be related to a range of factors including the larger population of individualized SWNT in these dispersions.

Due to the high degree of pristine MWNT aggregation in the cell medium, the uptake of pristine MWNTs was not quantified using UV spectroscopy, but qualitatively assessed using live-cell imaging, SEM and TEM. Consistent with light microscopy and SEM observations, TEM imaging revealed that pristine MWNT were mainly present as aggregates, and were often incompletely internalized by microglia after 72 hrs. While pristine MWNTs failed to affect microglial viability, pro-inflammatory cytokine release or NO production, a significant increase in ROS production was observed after 24 hrs. If the increased ROS can escape from within microglia cells, they can potentially induce damage, particularly to bystander cells in

the CNS such as neurons and astrocytes [55]. The majority of published studies consider the biodegradation of CNTs for bio-applications, which employ acid oxidized/functionalised CNTs [43]. However, as intrinsic properties of MWNTs become reduced during acid oxidation treatments, *pristine* nanotubes are preferable in many engineering applications such as electronics or composites, and so it is necessary to also consider pristine MWNTs in the case of accidental or occupational exposure. The current study clearly demonstrates differences in uptake of pristine MWNTs compared to AO MWNTs. Within the first three days of exposure, pristine MWNT aggregates are rarely broken down by phagocytic microglia, and incomplete internalisation is often observed after 72 hrs, leading to ROS generation.

In the case of 20 and 100 AO MWNTs, TEM imaging revealed that individual and small clusters of MWNTs were internalized by phagocytosis and piercing of the plasma membrane. Internalized AO MWNTs were observed in vesicles, multilaminar bodies and within the cell cytoplasm, but never in mitochondria nor in cell nuclei. The presence of 20 and 100AO MWNTs within the microglia cytoplasm without apparent cytotoxicity demonstrates an attractive opportunity for using MWNTs to deliver therapeutics to the brain. However, localisation of AO MWNTs in the cytoplasm as well as multilaminar bodies also has implications for the biostability of MWNTs in cells and tissues. Recently, many *in vitro* studies have simulated CNT biostability through exposure to enzymes, some for extended periods of time. Oxidised single walled nanotubes (ox-SWNTs) were found to disintegrate and lose their graphitic structure by enzymatic catalysis when incubated with horseradish peroxidase for 16 weeks at 4 ºC [56] or 10 days at RT [57], while the human neutrophil enzyme myeloperoxidase (hMPO) degraded ox-SWNTs after just 24 hrs [58]. However, oxidised MWNTs took significantly longer to degrade, with one report finding incomplete digestion after 60 days incubation with horseradish peroxidase in the presence of hydrogen

peroxide [59] and another finding a half-life of MWNTs of as long as 80 years [60]. The live-cell imaging in this work reveals the ability of microglia to disentangle and internalise AO MWNT aggregates. This process increases the proportion of the extracellular MWNT population which is able to enter *via* the phagocytic pathway, and hence the proportion of MWNTs which could potentially be degraded within oxidative environments in the microglia. However, the TEM imaging reported here also indicates that a portion of these MWNTs are able to escape from the phagolysosomal pathway, and sequester in the cell cytoplasm after as little as two hours exposure. While microglial cell death and subsequent phagocytosis may return these MWNTs to the phagolysosomal pathway in the long term, these observations suggest that *in vitro* enzymatic studies, which assume continual exposure to oxidative environments, may overestimate the degradation rates for MWNTs located in the cytoplasm, as well as those remaining in the extracellular space.

5. Conclusion

This study demonstrates the effects of MWNT functionalisation and aggregation state on internalisation and biostability in N9 microglia. Correlative live-cell and high-resolution imaging reveals dynamic processes of disentanglement of MWNT aggregates by microglia, for AO MWNTs but *not* pristine MWNTs. This disentanglement process is a crucial step in the internalisation of MWNT aggregates, and is expected to impact on the long term biodegradation and clearance of MWNTs. AO MWNT internalisation and cell association was determined by UV spectroscopy to be 52% ± 2% of 100AO MWNTs and 40% ± 3% of 20AO MWNTs interacting with N9 microglia after 24 hours. While AO MWNTs were readily internalized by microglia, neither pristine nor AO MWNTs affected cell viability or activation state after 24 hrs. However, the incomplete internalisation of pristine MWNTs resulted in increased ROS production. Taken together, our results show that the MWNT length and defectiveness must be controlled to achieve optimal and non-toxic delivery of

MWNT therapeutics, and also to increase the human safety of this class of nanomaterial. The balance between the amount of phagocytosed MWNTs and their escape from the phagolysosomal pathway into the cell cytoplasm has implications for the true degradation rates of AO MWNTs *in vivo*. More generally, the present results highlight the need for further correlative studies in other target organs to assess the role of MWNT aggregation on cellular uptake and biopersistence. Further work is especially relevant in the lung, where there is a risk of depositing MWNT aggregates through inhalation [61, 62], and therefore a need to determine the ability of alveolar macrophages to process extracellular MWNT aggregates.

Acknowledgements

The authors gratefully acknowledge funding from ERC starting investigator grant #257182. We thank Dr. Jeremy Skepper for his assistance with aggregate filtration, as well as Dr. David Payne and Dr. Anna Regoutz for their assistance with XPS measurements.

References

[1] Bhirde AA, Patel V, Gavard J, Zhang GF, Sousa AA, Masedunskas A, et al. Targeted Killing of Cancer Cells in Vivo and in Vitro with EGF-Directed Carbon Nanotube-Based Drug Delivery. Acs Nano. 2009;3:307-16.

[2] Kam NWS, O'Connell M, Wisdom JA, Dai HJ. Carbon nanotubes as multifunctional biological transporters and near-infrared agents for selective cancer cell destruction. P Natl Acad Sci USA. 2005;102:11600-5.

[3] Klumpp C, Kostarelos K, Prato M, Bianco A. Functionalized carbon nanotubes as emerging nanovectors for the delivery of therapeutics. Bba-Biomembranes. 2006;1758:404-12.

[4] Bussy C, Al-Jamal KT, Boczkowski J, Lanone S, Prato M, Bianco A, et al. Microglia Determine Brain Region-Specific Neurotoxic Responses to Chemically Functionalized Carbon Nanotubes. ACS Nano. 2015.

[5] Kafa H, Wang JTW, Rubio N, Venner K, Anderson G, Pach E, et al. The interaction of carbon nanotubes with an in vitro blood-brain barrier model and mouse brain in vivo. Biomaterials. 2015;53:437-52.

[6] Wang N, Feng Y, Zeng L, Zhao Z, Chen T. Functionalized Multiwalled Carbon Nanotubes as Carriers of Ruthenium Complexes to Antagonize Cancer Multidrug Resistance and Radioresistance. ACS Applied Materials & Interfaces. 2015;7:14933-45.

[7] Yang ST, Guo W, Lin Y, Deng XY, Wang HF, Sun HF, et al. Biodistribution of pristine single-walled carbon nanotubes in vivo. Journal of Physical Chemistry C. 2007;111:17761-4.

[8] Ren JF, Shen S, Wang DG, Xi ZJ, Guo LR, Pang ZQ, et al. The targeted delivery of anticancer drugs to brain glioma by PEGylated oxidized multi-walled carbon nanotubes modified with angiopep-2. Biomaterials. 2012;33:3324-33.

[9] Lee HJ, Park J, Yoon OJ, Kim HW, Lee DY, Kim DH, et al. Amine-modified single-walled carbon nanotubes protect neurons from injury in a rat stroke model. Nature Nanotechnology. 2011;6:120-4.

[10] Voge CM, Stegemann JP. Carbon nanotubes in neural interfacing applications. J Neural Eng. 2011;8.

[11] Al-Jamal KT, Gherardini L, Bardi G, Nunes A, Guo C, Bussy C, et al. Functional motor recovery from brain ischemic insult by carbon nanotube-mediated siRNA silencing. P Natl Acad Sci USA. 2011;108:10952-7.

[12] Gällentoft L, Pettersson LME, Danielsen N, Schouenborg J, Prinz CN, Linsmeier CE. Size-dependent long-term tissue response to biostable nanowires in the brain. Biomaterials. 2015;42:172-83.

[13] Bardi G, Tognini P, Ciofani G, Raffa V, Costa M, Pizzorusso T. Pluronic-coated carbon nanotubes do not induce degeneration of cortical neurons in vivo and in vitro. Nanomed-Nanotechnol. 2009;5:96-104.

[14] Kateb B, Van Handel M, Zhang L, Bronikowski MJ, Manohara H, Badie B. Internalization of MWCNTs by microglia: possible application in immunotherapy of brain tumors. Neuroimage. 2007;37 Suppl 1:S9-17.

[15] Sato Y, Yokoyama A, Shibata K, Akimoto Y, Ogino S, Nodasaka Y, et al. Influence of length on cytotoxicity of multi-walled carbon nanotubes against human acute monocytic leukemia cell line THP-I in vitro and subcutaneous tissue of rats in vivo. Molecular Biosystems. 2005;1:176-82.

[16] Sayes CM, Liang F, Hudson JL, Mendez J, Guo WH, Beach JM, et al. Functionalization density dependence of single-walled carbon nanotubes cytotoxicity in vitro. Toxicology letters. 2006;161:135-42.

[17] Wick P, Manser P, Limbach LK, Dettlaff-Weglikowska U, Krumeich F, Roth S, et al. The degree and kind of agglomeration affect carbon nanotube cytotoxicity. Toxicology letters. 2007;168:121-31.

[18] Poland CA, Duffin R, Kinloch I, Maynard A, Wallace WAH, Seaton A, et al. Carbon nanotubes introduced into the abdominal cavity of mice show asbestos-like pathogenicity in a pilot study. Nature Nanotechnology. 2008;3:423-8.

[19] Wang X, Xia T, Ntim SA, Ji ZX, Lin SJ, Meng H, et al. Dispersal State of Multiwalled Carbon Nanotubes Elicits Profibrogenic Cellular Responses That Correlate with Fibrogenesis Biomarkers and Fibrosis in the Murine Lung. Acs Nano. 2011;5:9772-87.
[20] Al-Jamal KT, Nunes A, Methven L, Ali-Boucetta H, Li SP, Toma FM, et al. Degree of Chemical Functionalization of Carbon Nanotubes Determines Tissue Distribution and Excretion Profile. Angewandte Chemie-International Edition. 2012;51:6389-93.
[21] Nunes A, Bussy C, Gherardini L, Meneghetti M, Herrero MA, Bianco A, et al. In vivo degradation of functionalized carbon nanotubes after stereotactic administration in the brain cortex. Nanomedicine. 2012;7:1485-94.
[22] Sato Y, Yokoyama A, Nodasaka Y, Kohgo T, Motomiya K, Matsumoto H, et al. Long-term biopersistence of tangled oxidized carbon nanotubes inside and outside macrophages in rat subcutaneous tissue. Sci Rep-Uk. 2013;3.
[23] Jin H, Heller DA, Strano MS. Single-particle tracking of endocytosis and exocytosis of single-walled carbon nanotubes in NIH-3T3 cells. Nano Lett. 2008;8:1577-85.
[24] Bertulli C, Beeson HJ, Hasan T, Huang YYS. Spectroscopic characterization of protein-wrapped single-wall carbon nanotubes and quantification of their cellular uptake in multiple cell generations. Nanotechnology. 2013;24:14.
[25] Holt BD, Dahl KN, Islam MF. Cells Take up and Recover from Protein-Stabilized Single-Wall Carbon Nanotubes with Two Distinct Rates. Acs Nano. 2012;6:3481-90.
[26] Kettenmann H, Hanisch UK, Noda M, Verkhratsky A. Physiology of Microglia. Physiol Rev. 2011;91:461-553.
[27] Verdejo R, Lamoriniere S, Cottam B, Bismarck A, Shaffer M. Removal of oxidation debris from multi-walled carbon nanotubes. Chemical Communications. 2007:513-5.
[28] Menzel R, Lee A, Bismarck A, Shaffer MSP. Inverse Gas Chromatography of As-Received and Modified Carbon Nanotubes. Langmuir. 2009;25:8340-8.
[29] Chen S. Cationic, anionic, and non-ionic water-soluble multiwalled carbon nanotubes, functionalised with minimal framework damage, for controlled biological investigations. in preparation.
[30] Ruenraroengsak P, Novak P, Berhanu D, Thorley AJ, Valsami-Jones E, Gorelik J, et al. Respiratory epithelial cytotoxicity and membrane damage (holes) caused by amine-modified nanoparticles. Nanotoxicology. 2012;6:94-108.
[31] Miranda KM, Espey MG, Wink DA. A rapid, simple spectrophotometric method for simultaneous detection of nitrate and nitrite. Nitric Oxide-Biol Ch. 2001;5:62-71.
[32] Tran MQ, Tridech C, Alfrey A, Bismarck A, Shaffer MSP. Thermal oxidative cutting of multi-walled carbon nanotubes. Carbon. 2007;45:2341-50.
[33] Chen S, Hu S, Smith EF, Ruenraroengsak P, Thorley AJ, Menzel R, et al. Aqueous cationic, anionic and non-ionic multi-walled carbon nanotubes, functionalised with minimal framework damage, for biomedical application. Biomaterials. 2014;35:4729-38.
[34] Muller KH, Motskin M, Philpott AJ, Routh AF, Shanahan CM, Duer MJ, et al. The effect of particle agglomeration on the formation of a surface-connected compartment induced by hydroxyapatite nanoparticles in human monocyte-derived macrophages. Biomaterials. 2014;35:1074-88.
[35] Righi M, Mori L, Delibero G, Sironi M, Biondi A, Mantovani A, et al. Monokine Production by Microglial Cell Clones. Eur J Immunol. 1989;19:1443-8.
[36] Stansley B, Post J, Hensley K. A comparative review of cell culture systems for the study of microglial biology in Alzheimer's disease. Journal of neuroinflammation. 2012;9:115.
[37] Li YY, Zhang T, Jiang YQ, Lee HF, Schwartz SJ, Sun DX. (-)-Epigallocatechin-3-gallate Inhibits Hsp90 Function by Impairing Hsp90 Association with Cochaperones in Pancreatic Cancer Cell Line Mia Paca-2. Mol Pharmaceut. 2009;6:1152-9.
[38] Miranda KM, Espey MG, Wink DA. A rapid, simple spectrophotometric method for simultaneous detection of nitrate and nitrite. Nitric oxide. 2001;5:62-71.

[39] Kushida T, Iijima H, Kushida H, Tsuruta C. En-Bloc Staining Available for Stereoscopic Observation of Epoxy-Resin Quetol-651-Embedded Thick Sections under a High-Voltage Transmission Electron-Microscope. Journal of Electron Microscopy. 1991;40:76-7.
[40] Luzzi DE, Smith BW. Electron irradiation effects in single wall carbon nanotubes. Journal of Applied Physics. 2001;90:3509-15.
[41] Cho J, Boccaccini AR, Shaffer MSP. The influence of reagent stoichiometry on the yield and aspect ratio of acid-oxidised injection CVD-grown multi-walled carbon nanotubes. Carbon. 2012;50:3967-76.
[42] Ferrari AC, Robertson J. Interpretation of Raman spectra of disordered and amorphous carbon. Physical Review B. 2000;61:14095-107.
[43] Heister E, Lamprecht C, Neves V, Tilmaciu C, Datas L, Flahaut E, et al. Higher Dispersion Efficacy of Functionalized Carbon Nanotubes in Chemical and Biological Environments. Acs Nano. 2010;4:2615-26.
[44] Pienaar IS, Harrison IF, Elson JL, Bury A, Woll P, Simon AK, et al. An animal model mimicking pedunculopontine nucleus cholinergic degeneration in Parkinson's disease. Brain Struct Funct. 2015;220:479-500.
[45] Oberdorster E. Manufactured nanomaterials (Fullerenes, C-60) induce oxidative stress in the brain of juvenile largemouth bass. Environ Health Persp. 2004;112:1058-62.
[46] Liu Z, Cai WB, He LN, Nakayama N, Chen K, Sun XM, et al. In vivo biodistribution and highly efficient tumour targeting of carbon nanotubes in mice. Nature Nanotechnology. 2007;2:47-52.
[47] Belyanskaya L, Weigel S, Hirsch C, Tobler U, Krug HF, Wick P. Effects of carbon nanotubes on primary neurons and glial cells. Neurotoxicology. 2009;30:702-11.
[48] Jeong B, Park JS, Lee KJ, Hong SC, Hyon JY, Choi H, et al. Direct measurement of the force generated by a single macrophage. Journal of the Korean Physical Society. 2007;50:313-9.
[49] Yu MF, Lourie O, Dyer MJ, Moloni K, Kelly TF, Ruoff RS. Strength and breaking mechanism of multiwalled carbon nanotubes under tensile load. Science. 2000;287:637-40.
[50] Demczyk BG, Wang YM, Cumings J, Hetman M, Han W, Zettl A, et al. Direct mechanical measurement of the tensile strength and elastic modulus of multiwalled carbon nanotubes. Mat Sci Eng a-Struct. 2002;334:173-8.
[51] Sammalkorpi M, Krasheninnikov A, Kuronen A, Nordlund K, Kaski K. Mechanical properties of carbon nanotubes with vacancies and related defects (vol 70, art no 245416, 2004). Physical Review B. 2005;71.
[52] Blighe FM, Lyons PE, De S, Blau WJ, Coleman JN. On the factors controlling the mechanical properties of nanotube films. Carbon. 2008;46:41-7.
[53] Lacerda L, Russier J, Pastorin G, Herrero MA, Venturelli E, Dumortier H, et al. Translocation mechanisms of chemically functionalised carbon nanotubes across plasma membranes. Biomaterials. 2012;33:3334-43.
[54] Geng J, Kim K, Zhang JF, Escalada A, Tunuguntla R, Comolli LR, et al. Stochastic transport through carbon nanotubes in lipid bilayers and live cell membranes. Nature. 2014;514:612-+.
[55] Block ML, Zecca L, Hong JS. Microglia-mediated neurotoxicity: uncovering the molecular mechanisms. Nat Rev Neurosci. 2007;8:57-69.
[56] Allen BL, Kichambare PD, Gou P, Vlasova, II, Kapralov AA, Konduru N, et al. Biodegradation of Single-Walled Carbon Nanotubes through Enzymatic Catalysis. Nano Lett. 2008;8:3899-903.
[57] Allen BL, Kotchey GP, Chen Y, Yanamala NVK, Klein-Seetharaman J, Kagan VE, et al. Mechanistic Investigations of Horseradish Peroxidase-Catalyzed Degradation of Single-Walled Carbon Nanotubes. Journal of the American Chemical Society. 2009;131:17194-205.
[58] Kagan VE, Konduru NV, Feng W, Allen BL, Conroy J, Volkov Y, et al. Carbon nanotubes degraded by neutrophil myeloperoxidase induce less pulmonary inflammation. Nature Nanotechnology. 2010;5:354-9.
[59] Russier J, Menard-Moyon C, Venturelli E, Gravel E, Marcolongo G, Meneghetti M, et al. Oxidative biodegradation of single- and multi-walled carbon nanotubes. Nanoscale. 2011;3:893-6.

[60] Fores-Cervantes DX, Maes HM, Schaffer A, Hollender J, Kohler HPE. Slow Biotransformation of Carbon Nanotubes by Horseradish Peroxidase. Environmental Science & Technology. 2014;48:4826-34.
[61] Kobler C, Poulsen SS, Saber AT, Jacobsen NR, Wallin H, Yauk CL, et al. Time-Dependent Subcellular Distribution and Effects of Carbon Nanotubes in Lungs of Mice. Plos One. 2015;10.
[62] Pauluhn J. Subchronic 13-Week Inhalation Exposure of Rats to Multiwalled Carbon Nanotubes: Toxic Effects Are Determined by Density of Agglomerate Structures, Not Fibrillar Structures. Toxicol Sci. 2010;113:226-42.

Supplementary Files

Click here to download Movie/Animation: Video1_100AO_48_hours.avi

Supplementary Files

Click here to download Movie/Animation: Video2_Pristine_48_hours.avi

Supplementary Files

Click here to download Supplementary Files: N9_Supplementary_refereed2.docx